



# The explosion characteristics of methane, hydrogen and their mixtures: A computational study



Mahdi Faghih<sup>a</sup>, Xiaolong Gou<sup>b</sup>, Zheng Chen<sup>a, b, \*</sup>

<sup>a</sup> SKLTCS, Department of Mechanics and Engineering Science, College of Engineering, Peking University, Beijing 100871, China

<sup>b</sup> Key Laboratory of Low-grade Energy Utilization Technologies and Systems, School of Power Engineering, Chongqing University, Chongqing 400044, China

## ARTICLE INFO

### Article history:

Received 30 September 2015

Received in revised form

18 December 2015

Accepted 18 December 2015

Available online 23 December 2015

### Keywords:

Deflagration index

Maximum pressure rise rate

Spherical flame propagation

Methane

Hydrogen

## ABSTRACT

The maximum pressure rise rate during gas explosions in enclosures and the deflagration index are important explosion characteristics of premixture. They can be used to quantify the potential severity of an explosion. However, there are large discrepancies in the deflagration index measured by different researchers for the same methane/air or hydrogen/air mixture. In this study, outwardly propagating spherical flames in a closed vessel are simulated by considering detailed chemistry as well as temperature-dependent thermal and transport properties. From simulation, the maximum pressure rise rate and deflagration index of methane, hydrogen and their mixtures are obtained. The influence of equivalence ratio, initial temperature and initial pressure on the maximum pressure rise rate and deflagration index is examined. It is found that the deflagration index has not been accurately measured in previous experiments, and that experiments conducted in cylindrical vessels have under-predicted greatly the deflagration index. For hydrogen/methane mixtures with hydrogen blending level above 70%, the deflagration index is observed to increase exponentially with hydrogen blending level. Moreover, the deflagration index is found to be greatly affected by initial pressure; while the initial temperature has little influence on deflagration index. Finally, based on theoretical analysis we propose a correlation to calculate the maximum pressure rise rate and deflagration index of methane at a broad range of initial pressure. The performance of this correlation is examined and it is demonstrated to provide accurate prediction.

© 2015 Elsevier Ltd. All rights reserved.

## 1. Introduction

Preventing unwanted explosion in fuels released into atmosphere is a crucial issue for fuel stocking and transportation. Therefore, the explosion characteristics of different fuels should be investigated thoroughly. The maximum pressure rise rate during gas explosions in enclosures,  $(dP/dt)_{\max}$ , and the deflagration index,  $K_G$ , are important explosion characteristics of premixture. They are popularly used to quantify the potential severity of an explosion. The maximum pressure rise rate,  $(dP/dt)_{\max}$ , depends not only on the mixture properties (such as mixture composition, initial temperature and initial pressure) but also on the volume of the vessel in which gas explosion takes place. Unlike  $(dP/dt)_{\max}$ , the deflagration index is an intrinsic property of the premixture and it is

independent of the volume of the vessel used in experimental measurements. The relationship between  $K_G$  and  $(dP/dt)_{\max}$  is

$$K_G = (dP/dt)_{\max} \times V^{1/3} \quad (1)$$

in which  $V$  is volume of combustion vessel.

Since the deflagration index is an intrinsic property of a premixture at certain conditions (i.e., at specified initial temperature and pressure), experiments conducted by different groups should provide nearly the same value of  $K_G$  for the same premixture at the same condition. Unfortunately, due to different sources of uncertainty, there are substantial discrepancies in the deflagration index measured by different researchers for the same methane/air or hydrogen/air mixture (see Table 1 and Table 2 presented in Section 4).

Almost all the experiments for deflagration index measurements were conducted in cylindrical or spherical vessels (Cammarota et al., 2010; Dahoe, 2005; Dahoe and de Goey, 2003; Holtappels, 2002; Ma et al., 2014; Movileanu et al., 2013; Razus

\* Corresponding author. SKLTCS, Department of Mechanics and Engineering Science, College of Engineering, Peking University, Beijing 100871, China.

E-mail address: [cz@pku.edu.cn](mailto:cz@pku.edu.cn) (Z. Chen).

et al., 2011; Salzano et al., 2012). When a cylindrical vessel is used, the unburned mixture cannot be completely consumed by the propagating spherical flame as it reaches the inner wall of the vessel. Therefore, both maximum pressure rise rate and deflagration index are underestimated in experiments using a cylindrical chamber. Ideally, a spherical chamber should be used to measure the deflagration index. Other factors affecting the accuracy of deflagration index measurement include flame instability and turbulence, which increase flame propagation speed and pressure rise rate. Stable flame propagation and laminar flow need to be ensured so that the deflagration index is not over-predicted (Cammarota et al., 2010; Razus et al., 2011). However, in large vessels the flame may become unstable due to hydrodynamic or thermal-diffusion instability and the initial laminar flow may become turbulent during the spherical flame propagation. Consequently, experiments conducted in large vessels over predict  $K_G$ . Furthermore, since both maximum pressure rise rate and deflagration index are strongly correlated with the flame propagation speed, those factors (e.g., mixture preparation, ignition, buoyancy and radiation) affecting flame propagation speed can also cause uncertainty in deflagration index measurement.

In simulation, the influence of different factors on flame propagation speed can be circumvented or minimized (Chen, 2015). Therefore, accurate deflagration index can be obtained from direct numerical simulation. In this study, outwardly propagating spherical flames in a closed spherical vessel are simulated by considering detailed chemistry as well as temperature-dependent thermal and transport properties. From simulation, the maximum pressure rise rate and deflagration index of methane, hydrogen and their mixtures are obtained. Methane is the main component of natural gas which is one of the promising clean alternative fuels. However, the low flame speed and narrow flammability limits of methane pose challenges for its utilization in combustion engines. To solve this problem, hydrogen addition is popularly used (Chen, 2009; Shrestha and Karim, 1999). However, hydrogen addition also increases the probability and strength of explosion. In the literature, several studies were conducted to measure the maximum pressure rise rate and deflagration index of methane (Cammarota et al., 2010; Crowl, 2010; Salzano et al., 2012), hydrogen (Ma et al., 2014; Salzano et al., 2012; Tang et al., 2009) and methane/hydrogen mixtures (Ma et al., 2014; Salzano et al., 2012).

The objectives of this study are to obtain the deflagration index of hydrogen, methane, and their mixtures, and to examine the effects of initial temperature, initial pressure and equivalence ratio on the deflagration index of hydrogen/methane mixtures. Furthermore, a correlation is proposed to calculate the maximum pressure rise rate and deflagration index of methane at a broad range of initial pressures.

## 2. Numerical methods

To get the maximum pressure rise rate and deflagration index, we have simulated one-dimensional (1D) spherical flame propagation in a closed spherical vessel using the in-house code, A-SURF (Chen, 2010; Chen et al., 2009; Dai and Chen, 2015). A-SURF solves the following conservation equations (including the unsteady Navier–Stokes equations as well as the energy and species conservation equations) for 1D, adiabatic, multicomponent, reactive flow in a spherical coordinate (Chen, 2010; Chen et al., 2009; Dai and Chen, 2015):

$$\frac{\partial U}{\partial t} + \frac{1}{r^2} \frac{\partial F(U)}{\partial r} = \frac{1}{r^2} \frac{\partial F_v(U)}{\partial r} + S_R \quad (2)$$

in which  $t$  and  $r$  are the temporal and spatial coordinates,

respectively. In Eq. (2), the vectors  $U$ ,  $F(U)$ ,  $F_v(U)$ , and  $S_R$  are defined as:

$$U = \begin{pmatrix} \rho Y_1 \\ \rho Y_2 \\ \vdots \\ \rho Y_n \\ \rho u \\ E \end{pmatrix}, F(U) = \begin{pmatrix} r^2 \rho u Y_1 \\ r^2 \rho u Y_2 \\ \vdots \\ r^2 \rho u Y_n \\ r^2 (\rho u^2 + P) \\ r^2 (E + P)u \end{pmatrix}, F_v(U) = \begin{pmatrix} -r^2 \rho Y_1 V'_1 \\ -r^2 \rho Y_2 V'_2 \\ \vdots \\ -r^2 \rho Y_n V'_n \\ r^2 \tau_1 \\ r^2 q \end{pmatrix}, S_R = \begin{pmatrix} \omega_1 \\ \omega_2 \\ \vdots \\ \omega_n \\ -2\tau_2/r \\ 0 \end{pmatrix} \quad (3)$$

in which  $\rho$ ,  $u$ ,  $P$ , and  $E$  denote density, flow velocity, pressure and the total energy per unit mass, respectively. The quantities,  $Y_k$ ,  $V'_k$  and  $\omega_k$ , are the mass fraction, diffusion velocity and production rate of species  $k$ , respectively. The production rate  $\omega_k$  due to chemical reaction is specified via collection of elementary reactions using a CHEMKIN compatible database (Kee et al., 1993). The mixture-averaged formula (Kee et al., 1985) is used to calculate diffusion velocity. In simulation the thermal diffusion of H and H<sub>2</sub> is considered since it affects the spherical flame propagation speed (Liang et al., 2013).

In the momentum equation, the viscous stresses,  $\tau_1$  and  $\tau_2$ , are:

$$\tau_1 = \frac{2\mu \partial u}{\partial r} - \frac{2\mu}{3r^2} \frac{\partial(r^2 u)}{\partial r}, \tau_2 = \frac{2\mu u}{r} - \frac{2\mu}{3r^2} \frac{\partial(r^2 u)}{\partial r} \quad (4)$$

where  $\mu$  is the dynamic viscosity of the mixture.

In the energy conservation equation, the total energy,  $E$ , is defined through:

$$E = -P + \rho u^2 / 2 + \rho h, h = \sum_{k=1}^n (Y_k h_k), h_k = h_{k,0} + \int_{T_0}^T C_{P,k}(T) dT \quad (5)$$

where  $T$  is the temperature,  $h_k$ , the enthalpy of species  $k$ ,  $h_{k,0}$  the species enthalpy of formation at the reference temperature  $T_0$ , and  $C_{P,k}$  the specific heat of species  $k$  at constant pressure. The heat flux in the energy conservation equation is

$$q = \lambda \frac{\partial T}{\partial r} - \rho \sum_{k=1}^n (h_k Y_k V'_k) \quad (6)$$

where  $\lambda$  is the thermal conductivity of the gas mixture.

The finite volume method is used to solve the conservation governing equations listed above. The Strang splitting fractional-step procedure is used to separate the time evolution of the stiff reaction term  $S_R$  from that of the convection and diffusion terms. In the first fractional step, the non-reactive flow is solved. The Runge–Kutta, MUSCL–Hancock, and central difference schemes, all of second-order accuracy, are used to calculate the temporal integration, convective flux, and diffusive flux, respectively. In the second fractional step, the homogeneous reaction at constant volume is solved using the VODE solver (Brown et al., 1989). Detailed chemistry is considered in simulation: the mechanism developed by Li et al. (2004) for pure hydrogen, and GRI-Mech 3.0 (Smith et al., 1999) for methane and methane/hydrogen mixtures. The chemical reaction rates as well as the thermodynamic and transport

properties are evaluated by using the CHEMKIN packages (Kee et al., 1993). A-SURF has been successfully used and validated in previous studies on spherical flame propagation, end-gas auto-ignition and detonation development (Chen, 2011, 2015; Yu and Chen, 2015; Yu et al., 2014; Zhang et al., 2012). More details on governing equations, numerical schemes, and code validation of A-SURF can be found in (Chen, 2010; Chen et al., 2009; Dai and Chen, 2015).

In simulation, a spherical chamber with inner radius of 5 cm is considered. The premixture is initially static at the specified initial temperature and pressure. Zero flow speed and zero gradients of temperature and mass fractions are enforced at both the center and wall boundaries. A small hot kernel (1–2 mm in radius) is used to initialize the spherical flame propagation from the center. The ignition effects on flame propagation are minimized through reducing the hot kernel size. In 1D simulation, the effects of instability and buoyancy are not included. Moreover, we only consider the adiabatic flame propagation and thereby the radiation effects are circumvented. To maintain adequate numerical resolution of the moving flame front, adaptive mesh refinement algorithm is used and the reaction front is always fully covered by finest meshes whose size is  $\Delta x = 4 \mu\text{m}$ . The correspond time step is  $\Delta t = 1 \text{ ns}$ . Numerical convergence has been checked and ensured by further decreasing the time step and mesh size in simulation.

To ensure that A-SURF can accurately predict the deflagration index, we have compared the pressure history predicted by A-SURF with those from experiments for stoichiometric  $\text{CH}_4/\text{air}$  mixtures in Fig. 1. Since the ignition time in simulation is not exactly the same as that in experiments, time-shifting is conducted to ensure that the pressure of  $P = 2.0 \text{ atm}$  occurs at the same time. Fig. 1 shows that very good agreement is achieved, indicating that the deflagration index obtained from present simulation is reliable. In Fig. 1, the deviation between experimental and simulation results at the end of combustion is caused by wall heat loss when the flame is close to the wall.

### 3. Theoretical analysis

Theoretical analysis of 1D spherical flame propagation in a closed spherical chamber is provided in this section. The analysis is

based on the following assumptions: 1) the 1D spherical flame is infinitely thin and smooth; 2) the pressure is spatially uniform and changes only with time; 3) the unburned gas is isentropically compressed; 4) both reactants and products are ideal gases; and 5) heat loss and buoyancy effects are negligible.

According to Bradley and Mitcheson (1976), the pressure rise rate,  $dP/dt$ , in a closed spherical vessel with the radius of  $R_W$  is:

$$\frac{dP}{dt} = \frac{3S_{u,e}\rho_u}{R_W\rho_{u,0}}(P_e - P_0) \left[ 1 - \left(\frac{P_0}{P}\right)^{1/\gamma_u} \frac{P_e - P}{P_e - P_0} \right]^{2/3} \quad (7)$$

where  $P$  is pressure,  $\rho$  is density, and  $S_u$  denotes the laminar flame speed. The subscripts, 0 and  $e$ , respectively refer to states before combustion (i.e., the initial states) and at the end of combustion (i.e., the equilibrium state). The subscript  $u$  denotes states of unburned gas. Ideally, maximum pressure rise rate occurs when the flame reaches the wall (i.e.,  $P = P_e$ ). Therefore, we have

$$\left(\frac{dP}{dt}\right)_{\max} = \frac{3S_{u,e}}{R_W} \times P_0 \times \left(\frac{P_e}{P_0} - 1\right) \times \left(\frac{P_e}{P_0}\right)^{1/\gamma_u} \quad (8)$$

in which the following correlation for adiabatic compression of unburned gas is used to eliminate the density ratio:

$$\rho_{u,e}/\rho_{u,0} = (P_e/P_0)^{1/\gamma_u} \quad (9)$$

In Eq. (9),  $\gamma_u$  is the specific heat capacity ratio of unburned gas.

The pressure ratio  $P_e/P_0$  is found to be nearly independent of the initial pressure. For example, the relative change in  $P_e/P_0$  is within 1.5% as  $P_0$  changes from 1 to 10 bar. Therefore, from Eq. (8) we have:

$$\left(\frac{dP}{dt}\right)_{\max} \propto P_0 S_{u,e} \quad (10)$$

Substituting Eq. (8) into Eq. (1) yields the following expression for deflagration index:

$$K_G = C_1 \times P_0 S_{u,e} \quad \text{with} \quad C_1 = 3 \left(\frac{4}{3}\pi\right)^{1/3} \left(\frac{P_e}{P_0} - 1\right) \left(\frac{P_e}{P_0}\right)^{1/\gamma_u} \quad (11)$$

According to the above discussion,  $C_1$  is nearly independent of the initial pressure. Since the laminar flame speed  $S_{u,e}$  depends on the initial pressure  $P_0$ , Eq. (11) indicates that  $K_G$  does not change linearly with  $P_0$ .

## 4. Results and discussion

### 4.1. Deflagration index of pure hydrogen and pure methane

The pressure history,  $P = P(t)$ , is recorded in 1D simulation of spherical flame propagation in a closed spherical chamber, and the deflagration index,  $K_G$ , is calculated according to Eq. (1). In Fig. 2, the deflagration index from simulation is compared with those from experiments for methane (Cashdollar and Hertzberg, 1985; Dahoe and de Goey, 2003; Gieras et al., 2006) and hydrogen (Cashdollar et al., 2000; Jo and Crowl, 2010; Schroeder and Holtappels, 2005; Tang et al., 2009) at normal temperature and pressure (NTP,  $T_{u,0} = 298 \text{ K}$  and  $P_0 = 1 \text{ atm}$ ). Besides, it also includes experimental results from Federal Institute for Material Research and Testing (Holtappels, 2002) which consists of experiments conducted by Federal Institute for Materials Research and Testing (BAM), Warsaw University of Technology (WUT), TU DELFT university and Institut national de l'environnement industriel et des risques (INERIS).

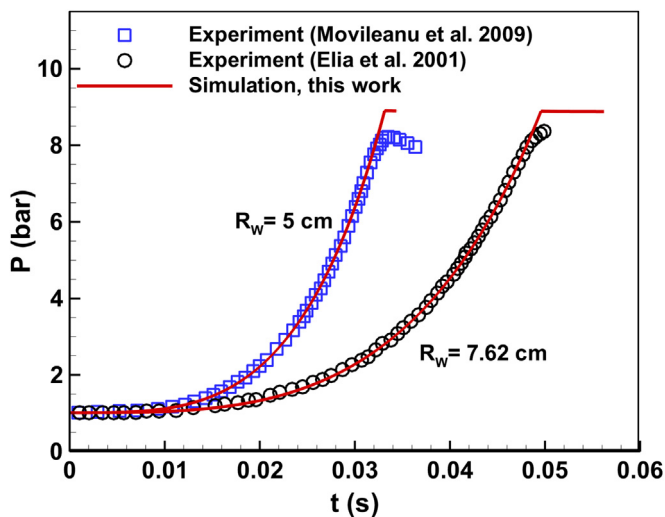
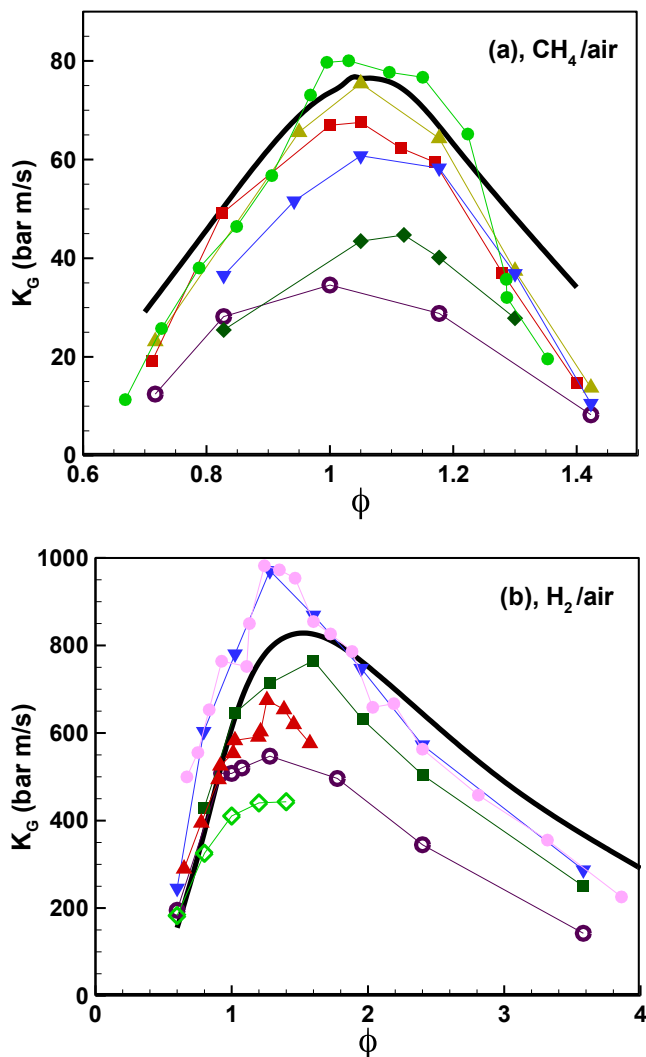


Fig. 1. Pressure evolution during combustion of stoichiometric  $\text{CH}_4/\text{air}$  at normal temperature and pressure (NTP,  $T_{u,0} = 298 \text{ K}$  and  $P_0 = 1 \text{ atm}$ ) in closed spherical chambers. The lines are results from simulation and the symbols stand for experimental results. It is noted that time-shifting has been conducted so that  $P = 2.0 \text{ atm}$  appears at the same time in experiments and simulations.



**Fig. 2.** Deflagration index as a function of equivalence ratio for (a) CH<sub>4</sub>/air and (b) H<sub>2</sub>/air at NTP. The thick lines are present simulation results; the filled symbols denote results from experiments using spherical chambers; and the unfilled symbols are results from experiments using cylindrical chambers. (a), unfilled purple circle: Gieras et al. (2006), the chamber volume is 40 L; filled dark green diamond: INERIS (2002), 20 L; filled yellow delta: TU DELFT university (2002), 20 L; filled red square: Cashdollar and Hertzberg (1985), 20 L; filled blue lower triangle: BAM (2002), 14 L; filled light green circle: Dahoe and de Goey (2003), 20 L. (b), unfilled purple circle: WUT (2002), 40 L; unfilled light green diamond: Tang et al. (2009), 5.3 L; filled blue lower triangle: BAM (2002), 14 L; filled dark green square: Schroeder and Holtappels (2005), 6 L; filled red delta: Cashdollar et al. (2000), 120 L; filled purple circle: Jo and Crowl (2010), 20 L. (For interpretation of the references to colour in this figure legend, the reader is referred to the web version of this article.)

Comparison between simulation and experimental results indicates that there are large discrepancies in the deflagration index measured by different researchers for the same methane/air or hydrogen/air mixture. Besides, for deflagration index most of experimental data are lower than simulation results. This is mainly due to heat loss to the wall which reduces the sharp pressure rise at the end of combustion (see Fig. 1). For methane, the closest experimental results to those from simulation were obtained in TU DELFT and by Cashdollar and Hertzberg (1985), both using a 20 L spherical vessel. For hydrogen, experimental data of Schroeder and Holtappels (2005), in 6 L vessel agrees well with those from simulation. For experiments conducted in a cylindrical chamber by Gieras et al. (2006), the deflagration

index is shown to be greatly under-predicted. As mentioned before, this is because the unburned mixture cannot be completely consumed by the propagating spherical flame as it reaches the inner wall of the vessel. Besides, Fig. 2(b) shows that some experiments provided larger deflagration index than simulation for lean and near stoichiometric H<sub>2</sub>/air mixtures. This might be caused by flame instability which accelerates flame propagation and thus increases maximum pressure rise rate and deflagration index.

The large discrepancies in the deflagration index measured by different researchers can be further demonstrated by experimental results for stoichiometric CH<sub>4</sub>/air and H<sub>2</sub>/air listed in Tables 1 and 2, respectively. For stoichiometric CH<sub>4</sub>/air, the reported deflagration index changes from 20 bar m/s measured in a 5 L cylindrical chamber (Cammara et al., 2010) to 90 bar m/s measured in a 120 L spherical chamber (Cashdollar et al., 2000). Even for deflagration index measured in the same 20 L spherical chamber, four different values of 86, 31.2, 70 and 39 bar m/s were obtained (Holtappels, 2002; Jo and Crowl, 2010; Ma et al., 2014). According to Tables 1 and 2, the deviation in deflagration index measured for stoichiometric CH<sub>4</sub>/air and H<sub>2</sub>/air reaches 350% and 411%, respectively. Therefore, there are substantial discrepancies in the deflagration index measurements.

#### 4.2. Deflagration index of hydrogen/methane mixtures

Numerical simulations have been conducted for hydrogen/methane mixtures. To quantify the hydrogen blending level, we introduce the variable,  $\alpha$ , which is defined as the volumetric percentage of hydrogen in the methane/hydrogen mixture. From pure methane to pure hydrogen,  $\alpha$  varies from 0 to 1. Fig. 3 depicts the deflagration index as a function of hydrogen blending level for stoichiometric CH<sub>4</sub>/H<sub>2</sub>/air at NTP. The experimental and simulation results from the literature (Ma et al., 2014; Salzano et al., 2012) are also plotted for comparison. It is observed that the deflagration index obtained from present simulation is higher than those from experiments. This is partly due to the fact that the adiabatic wall condition is considered in our simulation while wall heat loss occurs in experiments. Moreover, the present simulation results indicate that the change of the  $K_G$  against  $\alpha$  comprises two regimes: in the first regime with  $\alpha < 0.7$ ,  $K_G$  is insensitive to hydrogen addition and it only slightly increases with  $\alpha$ ; and in the second regime with  $\alpha > 0.7$ ,  $K_G$  increases exponentially with hydrogen blending level. This is mainly due to the influence of hydrogen addition on laminar flame speed,  $S_u$  (note that  $K_G$  is proportional to  $S_u$  according to Eq. (11)), as shown in Fig. 4. Though the equilibrium pressure,  $P_e$ , decreases with  $\alpha$ , the change in  $P_e$  is much less than that in  $S_u$ . Therefore, the exponential increase of  $K_G$  with  $\alpha$  is mainly caused by the similar change in  $S_u$  with  $\alpha$ .

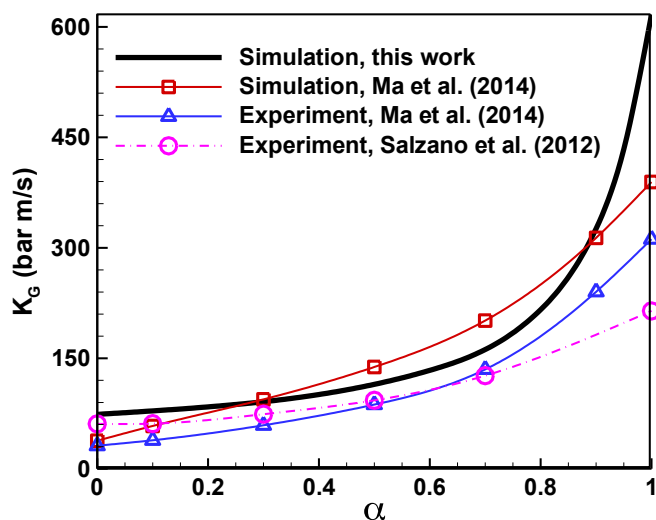
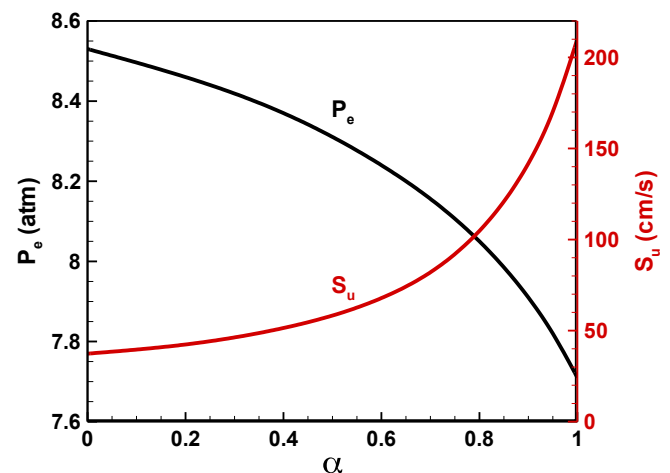
Fig. 3 only shows the results for stoichiometric mixture at NTP. Results at other conditions are also obtained from simulation and the effects of initial temperature, initial pressure and equivalence ratio on the deflagration index are examined. The results are presented in Fig. 5. Fig. 5(a) shows that the initial temperature has little influence on deflagration index. This is unexpected since the flame propagation speed increases dramatically with the initial temperature. However, besides the flame propagation speed, the equilibrium pressure,  $P_e$ , is also significantly affected by the initial temperature. For example, the increment of initial temperature from 298 K to 450 K for  $\alpha = 0.2$  decreases the equilibrium pressure from 8.46 atm to 5.72 atm. Consequently, as the initial temperature increases, the increase in  $S_u$  and decrease in  $P_e$  coincidentally balance with each other, which makes  $(dP/dt)_{max}$  and  $K_G$  to be nearly independent of the initial temperature

**Table 1**Deflagration index of stoichiometric CH<sub>4</sub>/air. The initial temperature and pressure are 298 K and 1 bar unless otherwise specified.

References	Deflagration index (bar m/s)	Vessel	Note
(Cammarota et al., 2010)	20	5 L cylinder	$T_{u,0} = 300$ K
(Gieras et al., 2006)	32.5 <sup>a</sup>	40 L cylinder	$T_{u,0} = 293$ K
(Crowl, 2010)	86	20 L sphere	
(Cashdollar et al., 2000)	68	20 L semi-sphere	
(Cashdollar et al., 2000)	90	120 L sphere	
(Bartknecht, 1981)	55	5 L sphere	
(Senecal and Beaulieu, 1998)	46	22 L cylinder	
(Ma et al., 2014)	31.2 <sup>a</sup>	20 L sphere	$T_{u,0} = 293$ K
(Salzano et al., 2012)	61 <sup>a</sup>	5 L cylinder	
BAM <sup>c</sup> (Holtappels, 2002)	65	14 L sphere	$K_G$ is presented at $\phi = 0.95$ & 1.05, for stoichiometric condition it is calculated by interpolation
TU DELFT university (Holtappels, 2002)	70	20 L sphere	$K_G$ is presented at $\phi = 0.95$ & 1.05, for stoichiometric condition it is calculated by interpolation
INERIS <sup>b</sup> (Holtappels, 2002)	39	20 L sphere	$K_G$ is presented at $\phi = 0.84$ & 1.05, for stoichiometric condition it is calculated by interpolation
Warsaw University of Technology (Holtappels, 2002)	34.5	40 L cylinder	

<sup>a</sup>  $K_G$  is not mentioned in the paper; it is calculated by using maximum pressure rise rate and cubic root law.<sup>b</sup> Institut national de l'environnement industriel et des risques.<sup>c</sup> Federal Institute for Materials Research and Testing.**Table 2**Deflagration index of stoichiometric H<sub>2</sub>/air. The initial temperature and pressure are 298 K and 1 bar unless otherwise specified.

References	Deflagration index (bar m/s)	Vessel	Note
(Cashdollar et al., 2000)	1100	120 L sphere	
(Senecal and Beaulieu, 1998)	638	22 L cylinder	
(Bartknecht, 1981)	550	5 L sphere	
NFPA 68 ("NFPA 68 (2007): Standard on Explosion Protection by Deflagration Venting,"; Senecal and Beaulieu, 1998)	659	5 L sphere	
(Ma et al., 2014)	312 <sup>a</sup>	20 L sphere	$T_{u,0} = 293$ K
(Salzano et al., 2012)	215 <sup>a</sup>	5 L cylinder	
(Tang et al., 2009)	410	5.3 cylinder	$T_{u,0} = 300$ K
BAM <sup>b</sup> (Holtappels, 2002)	640	6 L semi-sphere	
BAM <sup>b</sup> (Holtappels, 2002)	770	14 L sphere	
Warsaw University of Technology (Holtappels, 2002)	508	40 L cylinder	

<sup>a</sup>  $K_G$  is not mentioned in the paper; it is calculated by using maximum pressure rise rate and cubic root law.<sup>b</sup> Federal Institute for Materials Research and Testing.**Fig. 3.** Deflagration index as a function of hydrogen blending level for stoichiometric CH<sub>4</sub>/H<sub>2</sub>/air at NTP.**Fig. 4.** Equilibrium pressure,  $P_e$ , and laminar flame speed,  $S_u$ , as a function of hydrogen blending level for stoichiometric CH<sub>4</sub>/H<sub>2</sub>/air at NTP.

according to Eq. (8).

Fig. 5(b) compares the deflagration index at different initial pressures of 1, 2, 5 and 10 atm. It is observed that  $K_G$  increases with  $P_0$ . This is consistent with the theoretical correlation of Eq. (11).

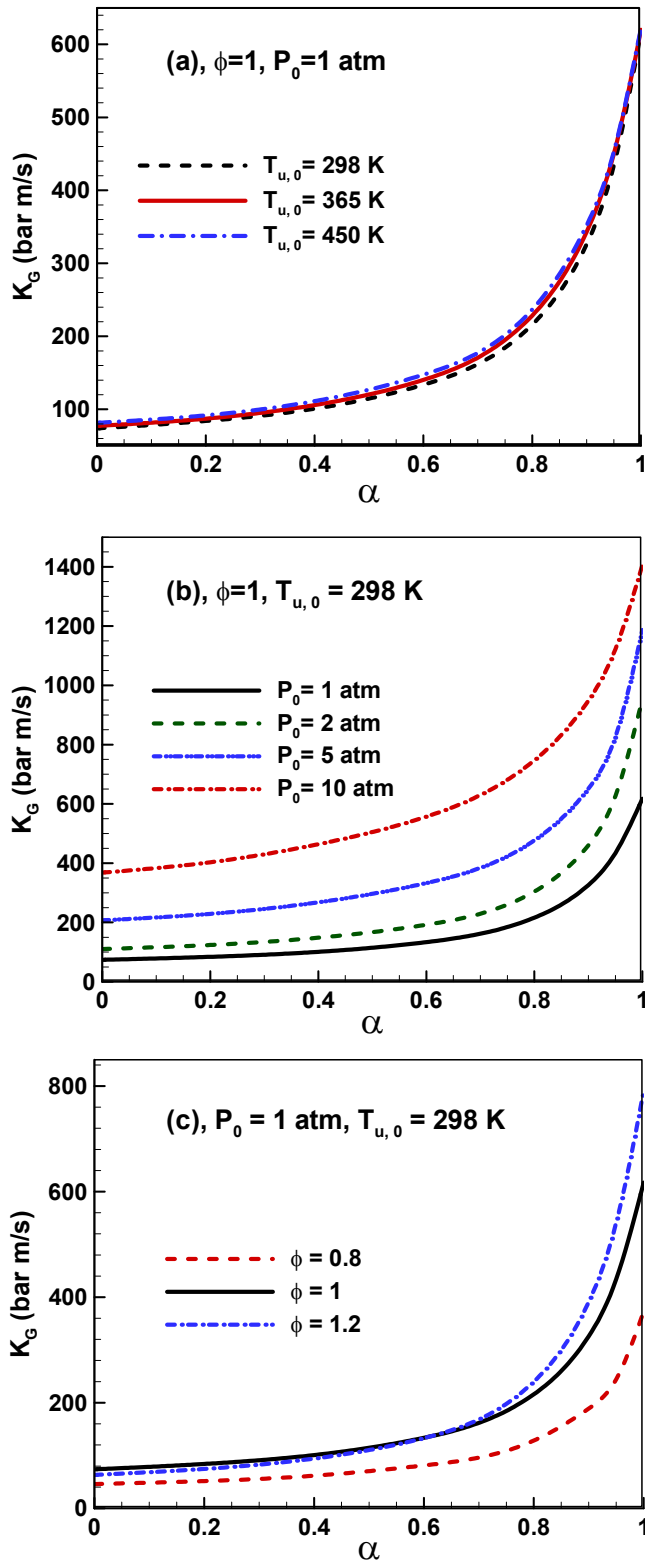


Fig. 5. Effect of initial temperature (a), initial pressure (b), and equivalence ratio (c) on the deflagration index of  $\text{CH}_4/\text{H}_2/\text{air}$  mixture.

Previous studies (Movileanu et al., 2013; Razus et al., 2011) found that  $K_G$  is linearly proportional to  $P_0$ . However, this is not correct since the laminar flame speed in Eq. (11) also depends on pressure. Further discussion on the pressure dependence of deflagration index will be presented in the next subsection.

The deflagration index of  $\text{CH}_4/\text{H}_2/\text{air}$  at NTP and different equivalence ratios is shown in Fig. 5(c). Similar trend in the change of  $K_G$  with  $\alpha$  is observed for these three equivalence ratios. For  $\phi = 0.8$ ,  $K_G$  is the smallest since the flame speed and equilibrium pressure are both the lowest. For  $\phi = 1$  and  $\phi = 1.2$ , the results are more complicated. For  $\alpha < 0.6$ ,  $K_G$  at  $\phi = 1$  is slightly larger than that at  $\phi = 1.2$ . This is because the mixture is methane dominant and it has larger peak flame speed and equilibrium pressure around  $\phi = 1$ . However, for  $\alpha > 0.6$ ,  $K_G$  at  $\phi = 1.2$  becomes larger than that at  $\phi = 1$ . This is due to the fact that the flame speed is higher at  $\phi = 1.2$  than at  $\phi = 1.0$  for hydrogen dominant mixtures. The results in Fig. 5(c) are consistent with those in Fig. 2 for pure methane and pure hydrogen.

#### 4.3. Pressure dependence of deflagration index

As mentioned before, the maximum pressure rise rate and deflagration index depend strongly on the initial pressure. Previous studies (Movileanu et al., 2013; Razus et al., 2011) demonstrated that both  $(dP/dt)_{\max}$  and  $K_G$  increase linearly with  $P_0$ . However, the linear relationship is not correct. Fig. 6 plots the maximum pressure rise rate as a function of initial pressure in logarithmic scale. The straight line is fitted to obtain the dependency of  $(dP/dt)_{\max}$  on  $P_0$ . Its slope is 0.7 in the logarithmic plot, indicating that  $(dP/dt)_{\max}$  is proportional to  $P_0^{0.7}$ . Therefore, the linear relationship between  $(dP/dt)_{\max}$  and  $P_0$  found in previous studies (Movileanu et al., 2013; Razus et al., 2011) is not correct for methane.

In the literature, different correlations have been proposed to calculate the maximum pressure rise rate or deflagration index (Cashdollar et al., 2000; Dahoe et al., 1996; Van den Bulck, 2005). Most of these correlations contain the laminar flame speed at the end of combustion,  $S_{u,e}$ , as an input, as indicated by Eq. (11). Unfortunately, it is difficult to measure  $S_{u,e}$  and thereby a correlation between laminar flame speed and initial temperature/pressure needs to be used to evaluate  $S_{u,e}$ . The laminar flame speed is usually correlated with the initial temperature and pressure in power law. In this work, the following relation obtained by Stone et al. (1998) is

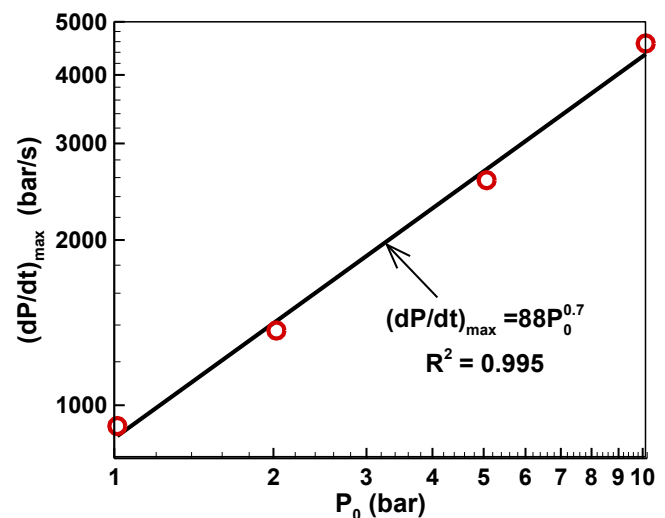


Fig. 6. Change of maximum pressure rise rate with the initial pressure in logarithmic scale for stoichiometric  $\text{CH}_4/\text{air}$  mixtures at  $T_{u,0} = 298 \text{ K}$ .

used for stoichiometric methane/air with the laminar flame speed in the unit of m/s:

$$S_u = 0.366 \left( \frac{T_u}{T_{u,0}} \right)^{1.42} \left( \frac{P}{P_0} \right)^{-0.297} \quad (12)$$

Substituting Eq. (12) into Eq. (8) yields the following correlation:

$$\begin{aligned} \left( \frac{dP}{dt} \right)_{\max} &= C_2 \cdot P_0^{0.703} \text{ with } C_2 \\ &= \frac{1.098}{R_W} \left( \frac{P_e}{P_0} - 1 \right) \left( \frac{P_e}{P_0} \right)^{(1.123\gamma_u - 0.42)/\gamma_u} \end{aligned} \quad (13)$$

Since  $P_e/P_0$  is nearly independent of the initial pressure as mentioned before, the coefficient  $C_2$  does not depend on  $P_0$ . The power of 0.703 in Eq. (13) is very close to the power of 0.7 obtained from curve fitting in Fig. 6. From Eqs. (1) and (13), we have the following correlation for deflagration index:

$$K_G = C_3 \cdot P_0^{0.703} \text{ with } C_3 = 1.770 \left( \frac{P_e}{P_0} - 1 \right) \left( \frac{P_e}{P_0} \right)^{(1.123\gamma_u - 0.42)/\gamma_u} \quad (14)$$

For stoichiometric methane/air with  $R_W = 5$  cm,  $T_0 = 298$  K,  $\gamma_u = 1.33$  and  $P_e/P_0 = 8.8$  ( $P_e/P_0$  changes from 8.75 to 8.86 for  $P_0$  from 1 atm to 10 atm), we have  $C_2 = 990.6$  and  $C_3 = 79.8$  according to their expressions in Eqs. (13) and (14).

To investigate the accuracy of Eq. (14), in Fig. 7 we plot the deflagration index predicted by different correlations as well as the results obtained from simulation and experiments results. Fig. 7(a) shows that there is large scatter among the experimental data. Again, the scatter in experimental data is mainly caused by different factors affecting the accuracy in deflagration index measurement. Nevertheless, the present correlation given by Eq. (14) matches well with present simulation results and experiment results obtained in a 20 L spherical chamber. The adiabatic simulation results from Ma et al. (2014) are shown to be unrealistically large. This might be caused by the one-step global reaction used in their simulation. Fig. 7(b) compares the results from different correlations with the present simulation results. To ensure fair comparison,  $S_{u,e}$  in all these correlations is calculated using Eq. (12). It is seen that only the results from the present correlation in Eq. (14) agrees well with the simulation results. Therefore, compared to previous correlations, the present correlation more accurately predicts the pressure-dependence of deflagration index for methane.

## 5. Conclusions

One-dimensional numerical simulation considering detailed chemistry and transport have been performed to investigate deflagration index of methane, hydrogen and their mixtures. The main conclusions are:

1. There are large discrepancies in the deflagration index measured for methane and hydrogen by different groups using different combustion chambers. Usually, the deflagration index measured in experiments is smaller than that obtained from simulation. This is mainly caused by wall heat loss or incomplete combustion in a cylindrical chamber. For methane/hydrogen mixtures, significant deviation between simulation and experimental results is observed at high hydrogen blending level.

2. The initial temperature and pressure have different impacts on the deflagration index. The deflagration index is almost unaffected by initial temperature; while it increases significantly with initial pressure. Based on theoretical analysis, a correlation is

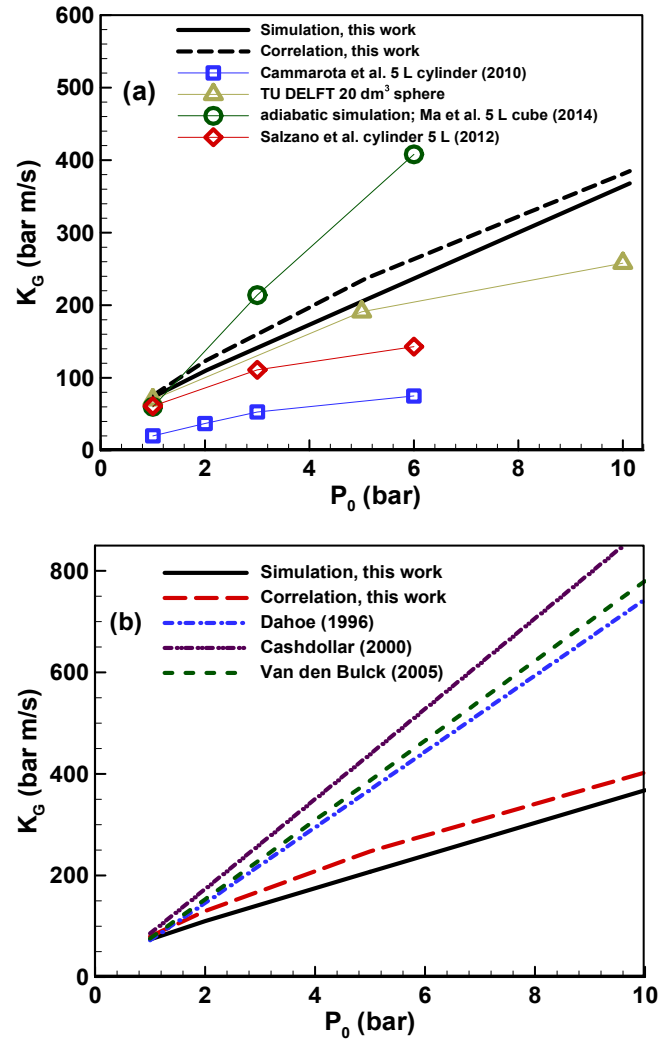


Fig. 7. Deflagration index as a function of initial pressure for stoichiometric  $CH_4/air$  mixtures at  $T_{u,0} = 298$  K: (a), comparison of present results with experimental results in the literature; and (b) comparison of present results with those predicted by different correlations proposed in the literature.

proposed to accurately predict the deflagration index of methane at a broad range of initial pressure. Moreover, it is demonstrated that for methane, the deflagration index (or maximum pressure rise rate) is proportional to the initial pressure to the power of 0.7. Therefore, the linear relationship between deflagration index and initial pressure proposed in previous studies is not correct.

## Acknowledgements

This work is supported by National Natural Science Foundation of China (Nos. 51322602 and 51136005). Z. C. also thanks the support from Key Laboratory of Low-grade Energy Utilization Technologies and Systems at Chongqing University (No. LLEUTS 201304).

## References

- Bartknecht, W., 1981. Explosions- Course, Prevention, Protection. Springer-Verlag, Berlin (Heidelberg).
- Bradley, D., Mitcheson, A., 1976. Mathematical solutions for explosions in spherical vessels. *Combust. Flame* 26, 201–217.
- Brown, P.N., Byrne, G.D., Hindmarsh, A.C., 1989. VODE: a variable-coefficient ODE solver. *SIAM J. Sci. Stat. Comput.* 10, 1038–1051.

- Cammarota, F., Di Benedetto, A., Russo, P., Salzano, E., 2010. Experimental analysis of gas explosions at non-atmospheric initial conditions in cylindrical vessel. *Process Saf. Environ.* 88, 341–349.
- Cashdollar, K.L., Hertzberg, M., 1985. 20-L Explosibility test chamber for dusts and gases. *Rev. Sci. Instrum.* 56, 596–602.
- Cashdollar, K.L., Zlochower, I.A., Green, G.M., Thomas, R.A., Hertzberg, M., 2000. Flammability of methane, propane, and hydrogen gases. *J. Loss Prev. Process Ind.* 13, 327–340.
- Chen, Z., 2009. Effects of hydrogen addition on the propagation of spherical methane/air flames: a computational study. *Int. J. Hydrogen Energy* 34, 6558–6567.
- Chen, Z., 2010. Effects of radiation and compression on propagating spherical flames of methane/air mixtures near the lean flammability limit. *Combust. Flame* 157, 2267–2276.
- Chen, Z., 2011. On the extraction of laminar flame speed and Markstein length from outwardly propagating spherical flames. *Combust. Flame* 158, 291–300.
- Chen, Z., 2015. On the accuracy of laminar flame speeds measured from outwardly propagating spherical flames: methane/air at normal temperature and pressure. *Combust. Flame* 162, 2442–2453.
- Chen, Z., Burke, M.P., Ju, Y.G., 2009. Effects of Lewis number and ignition energy on the determination of laminar flame speed using propagating spherical flames. *Proc. Combust. Inst.* 32, 1253–1260.
- Crowl, D.A., 2010. *Understanding Explosions*, vol. 16. John Wiley & Sons.
- Dahoe, A.E., 2005. Laminar burning velocities of hydrogen–air mixtures from closed vessel gas explosions. *J. Loss Prev. Process Ind.* 18, 152–166.
- Dahoe, A.E., de Goeij, L.P.H., 2003. On the determination of the laminar burning velocity from closed vessel gas explosions. *J. Loss Prev. Process Ind.* 16, 457–478.
- Dahoe, A.E., Zevenbergen, J.F., Lemkowitz, S.M., Scarlett, B., 1996. Dust explosions in spherical vessels: the role of flame thickness in the validity of the ‘cube-root law’. *J. Loss Prev. Process Ind.* 9, 33–44.
- Dai, P., Chen, Z., 2015. Supersonic reaction front propagation initiated by a hot spot in n-heptane/air mixture with multistage ignition. *Combust. Flame* 162, 4183–4193.
- Gieras, M., Klemens, R., Rarata, G., Wolański, P., 2006. Determination of explosion parameters of methane–air mixtures in the chamber of 40dm<sup>3</sup> at normal and elevated temperature. *J. Loss Prev. Process Ind.* 19, 263–270.
- Holtappels, K., 2002. Project SAFEKINEX, Contract No: EVG1-CT-2002–00072, Deliverable No. 8, Report on Experimentally Determined Explosion Limits, Explosion Pressures and Rates of Explosion Pressure Rise Part 1: Methane, Hydrogen and Propene.
- Jo, Y.-D., Crowl, D.A., 2010. Explosion characteristics of hydrogen–air mixtures in a spherical vessel. *Process Saf. Prog.* 29, 216–223.
- Kee, R.J., Grcar, J., Smooke, M., Miller, J., 1985. PREMIX: a Fortran Program for Modeling Steady Laminar One-dimensional Premixed Flames. Sandia Report SAND85–8240.
- Kee, R.J., Rupley, F., Miller, J., 1993. CHEMKIN-II: a FORTRAN Chemical Kinetics Package for the Analysis of Gas-Phase Chemical Kinetics. Sandia Report SAND89–8009B.
- Li, J., Zhao, Z., Kazakov, A., Dryer, F.L., 2004. An updated comprehensive kinetic model of hydrogen combustion. *Int. J. Chem. Kinet.* 36, 566–575.
- Liang, W., Chen, Z., Yang, F., Zhang, H., 2013. Effects of soot diffusion on the laminar flame speed and Markstein length of syngas/air mixtures. *Proc. Combust. Inst.* 34, 695–702.
- Ma, Q., Zhang, Q., Chen, J., Huang, Y., Shi, Y., 2014. Effects of hydrogen on combustion characteristics of methane in air. *Int. J. Hydrogen Energy* 39, 11291–11298.
- Movileanu, C., Razus, D., Oancea, D., 2013. Additive effects on the rate of pressure rise for ethylene–air deflagrations in closed vessels. *Fuel* 111, 194–200.
- NFPA 68, 2007. Standard on Explosion Protection by Deflagration Venting. National Fire Protection Association.
- Razus, D., Brinzea, V., Mitu, M., Movileanu, C., Oancea, D., 2011. Temperature and pressure influence on maximum rates of pressure rise during explosions of propane–air mixtures in a spherical vessel. *J. Hazard. Mater.* 190, 891–896.
- Salzano, E., Cammarota, F., Di Benedetto, A., Di Sarli, V., 2012. Explosion behavior of hydrogen–methane/air mixtures. *J. Loss Prev. Process Ind.* 25, 443–447.
- Schroeder, V., Holtappels, K., 2005. Explosion characteristics of hydrogen–air and hydrogen–oxygen mixtures at elevated pressures. In: *Proc. Intern. Conf. on Hydrogen Safety*, Pisa, Italy.
- Senecal, J.A., Beaulieu, P.A., 1998. KG: new data and analysis. *Process Saf. Prog.* 17, 9–15.
- Shrestha, S. o. B., Karim, G. a., 1999. Hydrogen as an additive to methane for spark ignition engine applications. *Int. J. Hydrogen Energy* 24, 577–586.
- Smith, G., Golden, D., Frenklach, M., 1999. The GRI-Mech 3.0 Chemical Kinetic Mechanism from. <http://combustion.berkeley.edu/gri-mech/>.
- Stone, R., Clarke, A., Beckwith, P., 1998. Correlations for the laminar-burning velocity of methane/diluent/air mixtures obtained in free-fall experiments. *Combust. Flame* 114, 546–555.
- Tang, C., Huang, Z., Jin, C., He, J., Wang, J., Wang, X., Miao, H., 2009. Explosion characteristics of hydrogen–nitrogen–air mixtures at elevated pressures and temperatures. *Int. J. Hydrogen Energy* 34, 554–561.
- Van den Bulck, E., 2005. Closed algebraic expressions for the adiabatic limit value of the explosion constant in closed volume combustion. *J. Loss Prev. Process Ind.* 18, 35–42.
- Yu, H., Chen, Z., 2015. End-gas autoignition and detonation development in a closed chamber. *Combust. Flame* 162, 4102–4111.
- Yu, H., Han, W., Santner, J., Gou, X., Sohn, C.H., Ju, Y., Chen, Z., 2014. Radiation-induced uncertainty in laminar flame speed measured from propagating spherical flames. *Combust. Flame* 161, 2815–2824.
- Zhang, W., Chen, Z., Kong, W., 2012. Effects of diluents on the ignition of premixed H<sub>2</sub>/air mixtures. *Combust. Flame* 159, 151–160.